The Airborne Cloud-Aerosol Transport System, Part I: Overview and Description of the Instrument and Retrieval Algorithms

John E. Yorks[1,3], Matthew J. McGill[2], V. Stanley Scott[2], Andrew Kupchock[3], Shane Wake[2], Dennis Hlavka[1], William Hart[1], Patrick Selmer[1]

[1]Science Systems and Applications, Inc. and NASA GSFC
[2]NASA GSFC
[3]University of Maryland - College Park

Abstract

The Airborne Cloud-Aerosol Transport System (ACATS) is a multi-channel Doppler lidar system recently developed at NASA Goddard Space Flight Center (GSFC). A unique aspect of the multi-channel Doppler lidar concept such as ACATS is that it is also, by its very nature, a high spectral resolution lidar (HSRL). Both the particulate and molecular scattered signal can be directly and unambiguously measured, allowing for direct retrievals of particulate extinction. ACATS is therefore capable of simultaneously resolving the backscatter/extinction properties and motion of a particle from a high altitude aircraft. ACATS has flown on the NASA ER-2 during test flights over California in June 2012 and science flights during the Wallops Airborne Vegetation Experiment (WAVE) in September 2012. This paper provides an overview of the ACATS method and instrument design, describes the ACATS retrieval algorithms for cloud and aerosol properties, and demonstrates the data products that will be derived from the ACATS data using initial results from the WAVE project. The HSRL retrieval algorithms developed for ACATS have direct application to future spaceborne missions such as the Cloud-Aerosol Transport System (CATS) to be installed on the International Space Station (ISS). Furthermore, the direct extinction and particle wind velocity retrieved from the

ACATS data can be used for science applications such as dust or smoke transport and convective outflow in anvil cirrus clouds.

1.0 Introduction

Current uncertainties in the role of aerosols and clouds limit our ability to accurately model the Earth's climate system and to predict climate change. There are several different types of lidar systems that can be used to measure cloud and aerosol properties and motion. Cloud-aerosol lidars measure the elastic backscatter from molecules and atmospheric particulates to resolve vertical profiles of spatial and optical properties of clouds and aerosols. The two most common elastic backscatter lidar techniques are standard backscatter lidars and high spectral resolution lidars (HSRL). The data provided by these lidar systems are essential to investigations of cloud and aerosol properties for numerous reasons. The vertical structure of cloud and aerosol layers resolved by lidar systems cannot be accurately obtained from passive satellite or passive airborne sensors. Furthermore, thin cloud optical depths are often below the detection limits of millimeter cloud radar systems (Comstock *et al.* 2002). In situ instruments can provide critical measurements of cloud and aerosol microphysical properties. However, they do not easily provide vertical profiles of these measurements and can alter the physical properties of the particles (Jensen *et al*. 2009; Zhao *et al.* 2011). Information obtained from cloud-aerosol lidar systems can improve knowledge of cloud and aerosol properties, which in turn advance parameterizations and reduce the uncertainties introduced in GCMs.

Standard elastic backscatter lidars are the least complex and most common lidar systems used to study vertical profiles of cloud and aerosol properties. Ground-based and airborne systems have been used in numerous field campaigns over the past few decades. In the last decade, as laser transmitters have become more reliable, the first space-based elastic backscatter lidar systems were designed and launched. The Geoscience Laser Altimeter System (GLAS; Spinhirne *et al.* 2005) was launched in January 2003 and the Cloud-Aerosol Lidar Infrared Pathfinder Satellite Observations project (CALIPSO; Winker *et al.* 2009) was launched in April 2006. These lidar systems fundamentally measure vertical profiles of attenuated total backscatter, without separation of particulate (Mie) and molecular (Rayleigh) scattering. There have been many methods developed to retrieve the particulate extinction and particulate backscatter coefficients from a cloud-aerosol lidar return signal. One technique is an inversion using standard backscatter lidar data developed by Fernald *et al*. (1972) and Klett (1981; 1985). The Klett or Fernald method makes it possible to solve the standard lidar equation by assuming a ratio of aerosol extinction to aerosol backscatter coefficients, referred to as the lidar ratio, is known and constant throughout a particulate layer. This assumption reduces the number of unknowns in the system to one. This method is commonly used to retrieve particulate extinction and backscatter coefficients from standard backscatter lidars such as CALIPSO (Young and Vaughan 2009) and the Cloud Physics Lidar (McGill *et al.* 2002). The lidar ratio (units of sr) is highly dependent on the optical and microphysical properties of atmospheric layer being measured. The lidar ratio typically varies from about 10 to 50 sr for tropospheric clouds (Del Guasta *et al*. 2001; Seifert *et al*. 2007; Yorks *et al*. 2011a) and from about 20 to 80 sr for aerosol particles (Ackermann 1998). For cloud and aerosol layers with an optical depth greater than 0.30, a 30 percent error in the assumed lidar ratio can lead to an error in the extinction retrieval from elastic backscatter lidar systems greater than 50 percent (Young *et al*. 2014).

Another method for retrieving the particulate backscatter and extinction coefficients from a lidar signal is a HSRL, which is based on the use of two measured profiles instead of only one. The HSRL technique utilizes the difference in spectral distribution of the molecular and particulate backscattered signals (Fiocco *et al.* 1971; Shipley *et al*. 1983; Grund *et al*. 1991). High spectral resolution optical filters are required to separate the particulate contribution from the molecular backscatter and resolve particulate extinction and backscatter coefficients independently with no assumption about the lidar ratio required. Only a few HSRL instruments have been successfully developed and operated to measure cloud and aerosol optical properties from ground or aircraft platforms. The iodine filter method (Piironen and Eloranta 1994) is the preferred method for HSRL systems to date. Recently airborne HSRL systems that employ iodine filters have been implemented and demonstrated on the NASA King Air (B-200) research aircraft (Hair *et al.* 2008) and the German Aerospace Center (DLR) Falcon research aircraft (Esselborn *et al.* 2008). However, a caveat of the iodine filter technique is that the actual particulate backscatter spectral broadening is not measured but inferred from the total and molecular backscatter. The backscattered signal also contains additional information that is imparted in the scattering process, such as the Doppler shift caused by the mean velocity of the particulate.

Doppler wind lidars use the frequency shift imparted on atmospheric aerosols and molecules to determine vertical profiles of the horizontal wind speed and direction. Providing these measurements on a global scale can progress understanding of atmospheric dynamics and improve numerical weather predictions (Baker *et al.* 1995). The two most common types of pulsed Doppler wind lidar systems are coherent (heteodyne) detection and direct (incoherent) detection. Coherent Doppler lidars use a heterodyning technique that mixes a pulsed lidar signal with a second laser signal to produce a beat frequency that is related to the Doppler shift. The second continuous laser beam is usually a local oscillator offset in frequency (Hall *et al.* 1984; Huffaker *et al.* 1984). Direct-detection lidars directly measure the frequency shift of the return signal using a high spectral resolution filter, such as a Fabry-Perot interferometer or etalon, and operate at shorter wavelengths than coherent systems (Benedetti-Michelangeli *et al.* 1972; Chanin *et al.* 1989; Garnier and Chanin 1992; Gentry and Korb 1994). One direct-detection method, termed multichannel (MC) by McGill and Spinhirne (1998), measures the Doppler shift by imaging the etalon fringe pattern onto a multiple element detector (Abreu *et al.* 1992; Fischer *et al.* 1995) The MC direct-detection concept requires the etalon transmission function to be aligned with the laser wavelength. This method was demonstrated by McGill *et al.* 1997a for a ground-based lidar developed at the University of Michigan.

A MC direct-detection Doppler lidar system capable of resolving the Doppler shifts inherent to atmospheric motions can simultaneously provide information about both the scattering intensity and the motion of the particle. Such an instrument was recently developed at NASA Goddard Space Flight Center (GSFC) called the Airborne Cloud-Aerosol Transport System (ACATS). ACATS is the first lidar system to simultaneously measure cloud/aerosol properties and wind from an airborne platform. The instrument has flown on the NASA ER-2 during test flights over California in June 2012 and as part of the Wallops Airborne Vegetation Experiment (WAVE) in September 2012. A description of the ACATS instrument design is provided, which includes details of the optical and mechanical components of the subsystems as well as the software that autonomously controls the instrument operation. This work advances the effort of McGill *et al*. 1997a and McGill *et al*. 1997b by demonstrating the retrieval algorithms for HSRL direct measurements of cloud and aerosol optical properties (i.e. extinction) that can be applied to future space-based HSRL missions. This study also presents initial ACATS HSRL results and data products from the WAVE campaign.

2.0 *ACATS Method and Instrument Description*

2.1 ACATS Methodology

The ACATS instrument is a multi-channel (MC) Doppler lidar system built for use on the NASA ER-2 high altitude aircraft. The MC technique passes the returned atmospheric backscatter through a single etalon and divides the transmitted signal into several channels (wavelength intervals), which are measured simultaneously and independently (Figure 1). The resulting aerosol spectral distribution is then compared to the outgoing laser distribution to infer the Doppler shift, as demonstrated in Figure 2a. Subsequent measurements of the atmospheric scattered light will reveal a wavelength offset that is proportional to the Doppler shift and directly related to the velocity of the scattering particles (Figure 2b). The basic concept is summarized in Figures 1 and 2. The MC method was demonstrated using the ground-based University of Michigan Doppler lidar (McGill *et al.* 1997a; McGill *et al.* 1997b).

A unique aspect of the MC Doppler lidar concept such as ACATS is that it is also a HSRL. Both the particulate and molecular scattered signal can be directly and unambiguously measured since the broad Rayleigh-scattered spectrum is imaged as a nearly flat background, illustrated in Figure 2c. The integral of the aerosol-scattered spectrum is analogous to the aerosol measurement from the typical absorption filter HSRL technique, providing exactly the same pieces of information as a standard HSRL (Figure 2d). While previous ground-based MC systems have been built and operated (Benedetti-Michelangeli *et al.* 1972; Abreau *et al.* 1992; McGill *et al.* 1997a), there has been no airborne demonstration of the technique and the method has not been used to derive HSRL cloud and aerosol properties.

2.2 ACATS Instrument Description

The ACATS instrument is composed of three main subsystems; laser transmitter, telescope, and receiver optics. A picture of the ACATS instrument fully assembled, with the receiver and telescope subsystems, is shown in Figure 3. A list of the ACATS instrument parameters is provided in Table 1. The instrument also includes a heating/cooling loop to provide stable thermal operation of the laser.

The frequency characteristics of pulsed lasers have recently been advanced due to the development of direct detection Doppler lidars and HSRLs. These techniques impose further requirements compared to standard backscatter lidars, such as lasers that are single frequency on a single pulse basis and more stable in time (central frequency drift of less than 1 MHz per minute). An injection-seeded, pulsed Nd:YAG laser was developed for the TWiLiTE instrument (Hovis *et al.* 2004) that achieves these frequency characteristics. This laser was later replicated for the ACATS instrument and provides a narrow wavelength distribution suitable for resolving the small frequency shifts due to the Doppler effect. The laser operates at an output power of about 10 mJ per pulse and repetition rate of 250 Hz at 532 nm and is designed for use in the low-pressure environment of high-altitude aircraft.

The ACATS telescope employs a rotating holographic optic element (HOE) to fit the small volume envelope of the ER-2 superpod and to enable vector wind measurements, which requires more than one viewing direction (Figure 3c). The telescope system is set for 45 degree off-nadir viewing and rotates on a bearing to permit step-stare operation. The number of scan angles (up to 8) and dwell time at each scan angle is controlled by software and can be modified before flight. A schematic of the optical design is presented in Figure 4. As the telescope rotates, the optical alignment changes and may lead to a loss in return signal if not corrected. A procedure that steps the telescope position using piezoelectric actuators and scans for the largest return signal is run during flight to determine the optical alignment at each scan position. The 8-inch diameter telescope is also fiber-coupled to the receiver subsystem to provide greatest flexibility.

The primary difference between a lidar system capable of only measuring total backscatter intensity (e.g., CALIOP or CPL) and an instrument that directly measures the particulate extinction and Doppler shift, such as ACATS, lies in the receiver subsystem (Figures 3b; 4). The heart of the ACATS receiver system is an etalon that provides the spectral resolution needed for the HSRL measurement and also to resolve the Doppler shift inherent in the backscattered signal. Backscattered light collected by the telescope is passed through the etalon and an image of the etalon fringe pattern is created. A bandpass filter is used in tandem with the etalon to reject background sunlight, permitting daytime operation. The optical gap of the etalon is 10 cm with an operational diameter of 35 mm and plate reflectivity of 85%. As with any MC system, it is critical to maintain the symmetry and shape of the etalon fringe pattern to avoid uncertainty in the measurement. A digital etalon controller was developed by Michigan Aerospace Corporation in which piezoelectric actuators control the etalon electronics to position and maintain the plate parallelism. Considerable work was performed to create autonomous flight software that maintains the etalon alignment over the entirety of an ER-2 flight. The signal transmitted by the etalon is then passed to the detector subsystem.

A holographic circle-to-point converter optic (McGill *et al.* 1997c; McGill and Rallison 2001) is placed in the focal plane to provide the spectral detection. The circle-to-point converter simplifies hardware requirements, improves efficiency of measuring the spectral content in the fringe pattern, and allows ACATS to utilize photon-counting detection. The holographic optic is coupled to a Hamamatsu H7260 linear array detector, which utilizes back-end electronics developed by Sigma Space Corporation to permit photon-counting detection at count rates in excess of 50 MHz. The ACATS receiver images ~1.2 orders over 24 detector channels. The ACATS etalon parameters result in a measurement dynamic range of ~400 m/s, more than sufficient for typical atmospheric motions.

An autonomous multi-channel data system is the final component of the instrument and was based entirely on work completed by Sigma Space Corporation in support of the CPL, UAV-CPL, and TWiLiTE lidars. The basis for the data system, the Advanced MultiChannel Scaler (AMCS) card, was first applied in the ER-2 CPL instrument. The data acquisition software is included in the data system and has its heritage in the CPL and UAV-CPL instruments. An important aspect of the ACATS data system, as developed for CPL and UAV-CPL, is the ability to downlink data in real-time from the aircraft using the onboard air and navigation payload server. The data system also incorporates a Novatel model OEMV-3RT2i GPS receiver and OEM-IMU-H58 inertial unit to enable accurate correction for platform motion. The Novatel system provides greater than 20 Hz update rates with 2 cm/s velocity accuracy. The raw ACATS data file consists of photon counts at each horizontal record (1 sec), range bin (30 m) and detector channel, which is then converted to atmospheric parameters such as backscatter and extinction coefficients.

2.3 ACATS Calibration Procedures

Several calibration parameters are required to accurately retrieve the wind velocity, aerosol and molecular backscatter from the ACATS data. These include normalization constants, instrument defect function parameter, and detector nonlinearity. The illumination and sensitivity of each detector channel are not the same, necessitating normalization constants to compensate. The detector normalization coefficients are determined using a white-light source to illuminate the telescope while the receiving optics remains unchanged. These normalization constants describe the relative response of the detector to broad bandwidth illumination.

The alignment of the circle-to-point converter (HOE) and Fabry-Perot fringe pattern also must be characterized. Each ring in the circle-to-point converter represents a detector channel. Since the circle-to-point converter and etalon are manufactured separately, a ring can have a dissimilar centricity and diameter compared to the fringe pattern projected onto it, resulting in signal loss to the corresponding detector channel. To complicate matters, this loss of signal can vary in each channel. In the case of ACATS the outer rings (higher detector channels) of the circle-to-point converter are not perfectly concentric with the fringe pattern, requiring normalization constants to compensate. The normalization coefficients are determined using the peak transmission of the etalon calibration data in each channel. Assuming perfect alignment in all channels, the peak transmission will remain constant as the signal is stepped through all detector channels. Thus, the ACATS channel with the highest transmission represents the best alignment, allowing all other channels to be normalized to the "best aligned" channel. These normalization constants describe the relative signal loss of the detector channel due to alignment imperfections.

To characterize the instrument defect parameter, an etalon calibration procedure has been developed for ACATS similar to the one outlined in McGill *et al*. (1997a). The etalon transmission equation as a function of detector channel (j) is expressed as (McGill 1996):

$$T(\Delta\lambda, j) = \sum_{n=0}^{\infty} A_n \cos\left[2\pi n\left(\frac{\Delta\lambda}{\Delta\lambda_{FSR}} + \frac{j}{N_{FSR}}\right)\right] \sin c\left(\frac{n}{N_{FSR}}\right) \qquad (2.3.1)$$

where $\Delta\lambda_{FSR}$ is the free spectral range and is defined as the change in wavelength necessary to change the order of interference by one. The free spectral range can also be represented by the number of channels necessary to change the order of interference by one, N_{FSR}. The function A_n is defined as:

$$A_n = 2\left(1 - \frac{\ell}{1-R}\right)^2 \left(\frac{1-R}{1+R}\right) R^n e^{-4\pi^2 n^2 \Delta d_D^2 \lambda_0^2} \qquad (2.3.2)$$

where ℓ is the loss of light due to absorption or scattering by the etalon plates and R is the plate reflectivity. The etalon transmission equation (2.3.1) is for an idealized etalon.

A real etalon function will be broadened by several effects, such as plate bowing, microscopic plate defects, detector broadening, and off-axis aberrations.

For the purpose of this study, it is sufficient to use an instrument defect parameter (Δd_D) to represent the etalon broadening effects and tune the etalon model so that it matches the measured ACATS spectral response. There are two important assumptions in determining the ACATS defect parameter. First, the defect parameter varies with detector channel to account for the variability of the etalon finesse with channel. It is also assumed that any broadening effects, and thus the etalon defect parameter, will follow a Gaussian distribution. The ACATS defect parameter is then determined by a calibration procedure similar to the one demonstrated in McGill *et al*. (1997a). Software runs a calibration procedure at least once per flight that varies the etalon gap using piezoelectric actuators. Varying the etalon gap moves the interference fringe pattern across the detector in 128 small steps, sampling nearly 3 orders (42 points per order). One can then determine the defect parameter for each channel by performing a least-squares fit to match the modeled etalon transmission function to the ACATS measured etalon response function using a similar technique to McGill *et al*. 1997a. The light source used to measure the ACATS etalon response is the same laser that is used for atmospheric measurements. Additionally, the calibration technique automatically compensates for any uncertainty in computing the laser bandwidth, since the laser width follows a Gaussian distribution similar to the etalon broadening term.

The measured ACATS spectrum can become distorted due to detector dead time and must be compensated for. All lidar systems that employ photon-counting detection experience this effect, which is a limitation on the number of photons that can be counted in a given time interval. For ACATS, the large near-field return pushes the detector into a nonlinear counting region. The nonlinear effects for this type of detector can be quantified by a detector dead time coefficient. This coefficient represents the fact that only one photon event can be counted at once, and the detector system has a certain time delta, or dead time, before it can count another. A typical Hamamatsu linear array detector, such as the one employed in ACATS, has a discriminator dead time of 65 to 75 ns for a discriminator maximum count rate on the order of 15 MHz. To improve this performance, the ACATS Hamamatsu linear array detector is customized with a discriminator built by Sigma Space Corporation under Small Business Innovative Research (SBIR) funding that has a shorter discriminator dead time. This permits photon-counting detection at count rates in excess of 40 MHz before there is a 10% reduction in observed count rate. The ACATS detector rarely experiences count rates higher than 10 MHz in atmospheric bins below 17 km (assuming an ER-2 altitude greater than 19 km). Therefore, the detector dead time coefficient is less than 1.05 for 99.5% of atmospheric bins with the exception of the near-field return.

3.0 *Development of ACATS Retrieval Algorithms*

ACATS provides data products similar to other cloud-aerosol lidars, HSRL systems, and Doppler wind lidars. The system is currently set for 45 degree off-nadir viewing and the telescope rotates to allow for two orthogonal line-of-sight (LOS) wind measurements, which are then used to compute vertical profiles of horizontal wind velocity and direction within particulate layers. The ACATS retrieval algorithms and data products for the horizontal wind velocity will be presented at a later date. This paper focuses on two types of aerosol/cloud products available from ACATS data that are directly applicable to the ISS CATS instrument. Standard backscatter products are computed similar to CPL and CALIPSO (McGill *et al.* 2007). HSRL products are produced at courser resolutions (450 m vertical and 5 km horizontal), but include direct retrievals of attenuated particulate backscatter, optical depth, as well as particulate extinction and backscatter coefficients. These products are similar to those produced by other HSRL systems.

3.1 Development of Standard Backscatter Algorithms

If the measured ACATS photon counts are summed over all channels as to neglect the spectral information provided by the etalon, vertical profiles of total backscatter can be retrieved from ACATS data. Similar to a standard backscatter lidar system (i.e. CALIOP), this total signal is composed of both the particulate scattering and molecular scattering. The standard lidar equation can be regrouped and solved for the attenuated total backscatter (ATB or γ), which has units of km^{-1} sr^{-1} and is defined as:

$$\gamma(\pi,r) = \left[\beta_M(\pi,r) + \beta_P(\pi,r)\right] * e^{-2\int_0^r \sigma(r')dr} \tag{3.1.1}$$

The molecular backscatter coefficient (β_M) is determined from Rayleigh scattering theory (Tenti *et al.* 1974; Young 1981) and is proportional to atmospheric density. Furthermore, the molecular extinction coefficient (σ_M) is resolved from the molecular backscatter coefficient though the relationship $\sigma_M(r) = \beta_M(\pi,r) * (8/3)\pi$. The ACATS standard ATB is computed using the standard lidar equation and calibrated by normalizing the signal to the molecular backscatter profile at high altitudes where aerosol loading is weakest (Russell *et al.* 1979; Del Guasta 1998). This calibration technique is the well-accepted method of calibrating backscatter lidar signals and is used in CALIPSO and CPL retrievals (McGill *et al*. 2007). ACATS cloud and aerosol layer boundaries are determined using a similar method to CPL (Yorks *et al*. 2011b). The advantage of using this retrieval scheme is that the particulate layer properties can be obtained at higher resolutions, both vertically and horizontally, than using the HSRL retrieval algorithms. Therefore, this “standard” lidar method is used to compute ACATS attenuated total backscatter, as well as cloud and aerosol layer boundaries at a vertical resolution of 40 m and horizontal resolution of 400 m (2 sec).

3.2 ***Development of HSRL Algorithms***

The ACATS HSRL retrieval algorithms are unique and different compared to the algorithms of current iodine filter HSRL systems (Hair *et al.* 2008). The inclusion of an etalon in the ACATS instrument design results in a more complicated ACATS lidar equation compared to the standard lidar equation and iodine filter HSRL equations. The etalon transmission function (Equation 2.3.1) is convolved with the standard backscatter lidar equation to yield the expression for the number of photon counts detected per channel (j), as derived in McGill 1996:

$$\begin{aligned} N(r,j) &= \frac{E_T\lambda}{hc}O_A(r)\frac{A_T}{4\pi r^2}\Delta r Q_E T_O T_F(\lambda)\frac{\eta(j)}{n_C} \\ &\times\sum_{n=0}^{\infty}A_{n,j}\mathrm{sinc}\left(\frac{n}{N_{FSR}}\right)\exp\left(\frac{-\pi^2 n^2\Delta\lambda_L^2}{\Delta\lambda_{FSR}^2}\right)\left[\alpha(r)+\omega(r)\exp\left(\frac{-\pi^2 n^2\Delta\lambda_M^2}{\Delta\lambda_{FSR}^2}\right)\right] \\ &\times\cos\left[2\pi n\left(\frac{\lambda_0-\lambda_C}{\Delta\lambda_{FSR}}-\frac{2U_{LOS}(r)\lambda_0\sin\varphi}{c\Delta\lambda_{FSR}}-\frac{j}{N_{FSR}}\right)\right] \end{aligned} \quad (3.2.1)$$

The first term represents the instrument parameters and the definitions of individual parameters are shown in Table 2. The second term contains the laser broadening ($\Delta\lambda_L$), molecular broadening ($\Delta\lambda_M$), and the atmospheric physics. The attenuated particulate backscatter (α) and attenuated molecular backscatter (ω) are expressed as:

$$\omega(\pi,r) = \beta_M(\pi,r) * e^{-2\int_0^r \sigma(r')dr} \tag{3.2.2}$$

$$\alpha(\pi,r) = \beta_P(\pi,r) * e^{-2\int_0^r \sigma(r')dr} \tag{3.2.3}$$

The Doppler shift is characterized by the second part of the third term, where U_{LOS} is the LOS wind velocity in ms^{-1}. The attenuated particulate backscatter, attenuated molecular backscatter, and LOS wind velocity are the three unknown variables in Equation 3.2.1. Since there are 24 detector channels, the ACATS system is an over-determined set of equations. These three unknowns are determined using a method developed by McGill *et al*. (1997b). First, the ACATS lidar equation (Equation 3.2.1) is linearized by expanding the relevant variables in a Taylor series. The equation is then written in matrix form:

$$\begin{bmatrix} N_1 - N_{0,1} \\ \cdot \\ \cdot \\ N_{24} - N_{0,24} \end{bmatrix} = \begin{bmatrix} \left.\frac{\partial N_1}{\partial U_{LOS}}\right|_{U_{LOS,0}} & \left.\frac{\partial N_1}{\partial \alpha}\right|_{\alpha_0} & \left.\frac{\partial N_1}{\partial \omega}\right|_{\omega_0} \\ \cdot & \cdot & \cdot \\ \cdot & \cdot & \cdot \\ \left.\frac{\partial N_{24}}{\partial U_{LOS}}\right|_{U_{LOS,0}} & \left.\frac{\partial N_{24}}{\partial \alpha}\right|_{\alpha_0} & \left.\frac{\partial N_{24}}{\partial \omega}\right|_{\omega_0} \end{bmatrix} \begin{bmatrix} U_{LOS} - U_{LOS,0} \\ \alpha - \alpha_0 \\ \omega - \omega_0 \end{bmatrix} \tag{3.2.4}$$

This equation can also be written as:

$$\Delta N = G\Delta x \tag{3.2.5}$$

An iterative weighted least-squares fitting technique is employed to resolve these three parameters and their corresponding uncertainty, in which the solution is:

$$\Delta x^{est} = \left(G^T W G\right)^{-1} G^T W \Delta N \tag{3.2.6}$$

where W is the weighting matrix and G is the generalized matrix to be inverted. The solution for the molecular and particulate signals are linear, but non-linear for the Doppler shift. This least-squares fit method was tested and proven by McGill *et al*. (1997b) to retrieve the horizontal wind velocity. This work advances the effort of McGill *et al*. (1997a) and McGill *et al*. (1997b) by developing HSRL retrievals of cloud and aerosol properties. The first step is to compute the molecular backscatter coefficient (β_M) and two-way transmission (T_M^2) from Rayleigh scattering theory and meteorological data from a nearby radiosonde. The definition for the attenuated molecular backscatter (Eq. 3.2.2) can be rewritten in terms of the two-way transmission, corrected for the slant path, and solved for the two-way particulate transmission (T_p^2):

$$T_P^2(r) = \left[\frac{\omega(\pi,r)}{\beta_M(\pi,r)T_M^2(r)}\right]^{\cos\theta} \tag{3.2.7}$$

Therefore, the two-way particulate transmission can be determined without making unnecessary assumptions about the lidar ratio, as in the Klett or Fernald method (Fernald *et al.* 1972; Klett 1981, 1985). Once T_p^2 is known, the definition of the attenuated particulate backscatter (Eq. 3.2.3) can be rewritten and used to directly retrieve the particulate backscatter coefficient (β_P):

$$\beta_P(\pi,r) = \frac{\alpha(\pi,r)}{T_M^2(r)T_P^2(r)} \tag{3.2.8}$$

The particulate optical depth is then:

$$\tau_P(r) = -\frac{1}{2}\ln\left[T_P^2(r)\right] \tag{3.2.9}$$

The particulate extinction coefficient (σ_P) is directly retrieved using the equation:

$$\sigma_P(r) = \frac{\partial \tau_P(r)}{\partial r} \quad (3.2.10)$$

and the particulate lidar ratio is:

$$S_P(r) = \frac{\sigma_P(r)}{\beta_P(r)} \quad (3.2.11)$$

This method is used to compute profiles and layer-integrated values of the aforementioned variables at a vertical resolution of 450 m and horizontal resolution of 5 km (25 sec). Their corresponding uncertainties are computed using propagation of errors. If high-resolution optical properties are desired, the directly retrieved lidar ratio can be utilized as a parameterization to compute high-resolution optical properties using the Klett or Fernald method.

4.0 *Initial Results from WAVE Campaign*

During the period of 9 to 27 September 2012, ER-2 aircraft flights were conducted out of Wallops Island, VA as part of the WAVE project. These flights were planned over land, targeting specific land and vegetation surfaces with a scientific objective of simulating Ice, Cloud and land Elevation Satellite 2 (ICESat-2) data using the Multiple Altimeter Beam Experimental Lidar (MABEL; McGill *et al*. 2013). ACATS was a payload on a total of 13 ER-2 flights, which included observations of thin cirrus clouds, and smoke layers. During these flights, software directed the ACATS telescope to rotate counter-clockwise to four look angle positions denoted by azimuth angle relative to the aircraft nose: 0º (fore), 90º (right), 180º (aft), and 270º (left). At each look angle, the dwell time was set for 60 seconds. The WAVE campaign represents the first science flights for the ACATS instrument in which the telescope rotated and more than one look angle was used. Due to limited time before the project, the telescope alignment was optimized only at the 270-degree look angle. The telescope alignment for the other three look angles was performed in the field using the new and untested in-flight telescope alignment procedure. Portions of flights, and in some cases entire flights, were used to test and refine the etalon calibration procedure and telescope alignment. Furthermore, only two look angles were used for some flights if proper telescope alignment was not achieved at all four look angles. An example of the photon counts summed across all 24 detector channels at each of the four look angles from the 26 September 2012 flight is shown in Figure 5 and demonstrates the ability of ACATS to observe cirrus clouds (between 10 and 12 km) at multiple look angles. Overall, ACATS collected science data with high signal-to-noise ratio (SNR) in at least one look angle during 8 of the 13 total flights. The telescope alignment and LOS wind retrievals will be improved before future ACATS flights. This study will focus on ACATS retrievals of cloud and aerosol properties from the WAVE project, particularly those at the 270-degree look angle and high quality data from the other look angles.

There were several flights during WAVE in which ACATS collected quality data at multiple look angles. Perhaps the best ACATS performance was on the 26 September ferry flight back to Palmdale, CA when all four look angles were well aligned. Figure 6 shows the 532 nm ATB (km^{-1} sr^{-1}) computed using the standard method (a), the Attenuated Particulate Backscatter (km^{-1} sr^{-1}) using the HSRL method (b), and the directly-retrieved Particulate Extinction Coefficient (km^{-1}) at the 0 degree look angle (c) for the flight on 26 September 2012. Clearly visible in these images are cloud layers observed by ACATS as the ER-2 flew over the Ohio River Valley (20:28:05 to 21:30:00 UTC) and over North Dakota (about 00:24:10 UTC). ACATS also measured a large smoke plume (00:24:10 to 02:10:00 UTC) that extended as high as 6 km over Montana. The images in Figure 6 demonstrate the typical ACATS cloud and aerosol data products. The extinction and backscatter values are typical for cloud and smoke layers and appear to be similar across retrieval methods.

The ACATS telescope alignment on the 14 Sep. flight at the 270 degree look angle was the best for the entire campaign, making it a good case to assess biases in the two retrieval methods. Figure 7 shows the 532 nm ATB computed using the standard method (a) and using the HSRL method (b). The latter is essentially $\alpha + \omega$. Cirrus clouds between 9 and 13 km are observed throughout the flight. Figure 8 shows the mean profiles of 532 nm ATB computed using the standard method (blue) averaged to the resolutions of the HSRL products, as well as the ATB using the HSRL method (red) for the grey shaded box in Figure 7b centered around 22:32:22 UTC. Both ATB profiles follow the modeled molecular profile closely above the cirrus layer and show similar structure inside the cirrus layer. The standard ATB retrieval is about 10 percent higher than the ATB computed using the HSRL method within the cirrus layer. This difference is likely due to the errors in the calibration technique used in both retrievals. The error in the CPL calibration constant is estimated to be around 5 percent at 532 nm due to signal noise and the presence of aerosols in the CPL calibration zone (Campbell *et al*., 2008; Vaughan *et al*. 2010). Errors in the determination of the etalon defect parameter can lead to errors of as much as 5 percent in the HSRL retrieved attenuated molecular and particulate backscatter. Although this comparison provides confidence in the ACATS HSRL algorithms, it does not resolve any possible instrument biases. To address this issue, the ACATS standard backscatter and HSRL products are compared to coincident CPL cloud and aerosol properties during the WAVE campaign in a companion paper.

5.0 Summary

A new multi-channel direct-detection Doppler wind lidar has been developed at NASA GSFC for use on the NASA ER-2 called the Airborne Cloud-Aerosol Transport System (ACATS). ACATS employs a Fabry-Perot interferometer to provide the spectral resolution needed to retrieve the Doppler shift, similar to the ground-based University of Michigan MC direct-detection Doppler wind lidar (McGill *et al.* 1997a). The ACATS instrument design includes a seeded laser and circle-to-point converter, as well as a heating/cooling loop for stable laser performance during airborne operation. The ACATS telescope rotates to four look angles to permit the retrieval of the horizontal wind velocity within atmospheric layers. ACATS also advances the technology of a MC direct-detection Doppler wind lidar by demonstrating the utility of such an instrument for HSRL retrievals of cloud and aerosol properties.

The nature of a MC direct-detection Doppler wind lidar such as ACATS permits three types of cloud and aerosol lidar retrievals: standard backscatter lidar products such as ATB and layer boundaries, directly retrieved cloud and aerosol optical properties such as extinction and lidar ratio using the HSRL technique, and horizontal wind velocity of the cloud or aerosol particles within an atmospheric layer. This paper outlines the retrieval algorithms for all two of these types of ACATS data products, focusing on the HSRL derived cloud and aerosol properties. The first ACATS science flights were conducted during the WAVE project in September 2012. Initial results demonstrate the effectiveness of ACATS as an airborne HSRL system. The HSRL ATB retrieval for cirrus observed during the 14 September flight at the 270-degree look angle agrees with the ATB derived using the standard backscatter method to within 10 percent. Since the ISS CATS HSRL receiver is designed similar to ACATS, the algorithms and data products developed for ACATS have direct application to this future spaceborne mission Furthermore, the ACATS HSRL and wind products can be used for science applications such as aerosol transport, smoke plume properties and convective outflow in tropical storms.

Acknowledgments

NASA's Earth Science Technology Office (ESTO) Advanced Component Technology (ACT) program funded the development of the ACATS receiver subsystem. NASA's Airborne Instrument Technology Transfer (AITT) program funded ACATS instrument integration and ER-2 test flights. A special thanks to all the engineers at Sigma Space Corporation that were involved in building ACATS. We also thank Russ Dickerson for valuable discussions.

References

Abreu, V. J., J. E. Barnes, and P. B. Hays, 1992: Observations of winds with an incoherent lidar detector, *Appl. Opt*., **31**, 4509–4514.

Ackermann J., 1998: The extinction-to-backscatter ratio of tropospheric aerosol: numerical study. *J. Atmos. Oceanic Technol.*, **15**, 1043–1050.

Baker, W, and Coauthors, 1995: Lidar-measured winds from space: a key component for weather and climate prediction. *BAMS*, **76**, 869-888

Benedetti-Michelangeli, G., F. Congeduti, and G. Fiocco, 1972: Measurement of aerosol motion and wind velocity in the lower troposphere by Doppler optical lidar, *J. Atmos. Sci*., **29**, 906–910.

Chanin, M. L., A. Garnier, A. Hauchecorne, and J. Porteneuve, 1989: A Doppler lidar for measuring winds in the middle atmosphere, *Geophys. Res. Lett*., **16**, 1273–1276.

Comstock, J. M., T. P. Ackerman, and G. G. Mace, 2002: Groundbased lidar and radar remote sensing of tropical cirrus clouds at Nauru Island: Cloud statistic and radiative impacts. *J. Geophys. Res*., **107**, 4714, doi:10.1029/2002JD002203.

Del Guasta, M., 1998: Errors in the retrieval of thin-cloud optical parameters obtained with a two-boundary algorithm, Appl. Opt., 37, 5522–5540.

Esselborn, M., M. Wirth, A. Fix, M. Tesche, and G. Ehret, 2008: Airborne high spectral resolution lidar for measuring aerosol extinction and backscatter coefficients. *Appl. Opt*, **47**, 346– 358.

Fernald, F.G., B. M. Herman and J. A. Reagan, 1972: "Determination of aerosol height distributions with lidar", *Journal of Applied Meteorology*, **11**, 482-489.

Fiocco, G., G. Beneditti-Machelangeli, K. Maschberger, and E. Madonna, 1971: *Nature Phys. Sci*., **229**, 78.

Fischer, K. W., V. J. Abreu, W. R. Skinner, J. E. Barnes, M. J. McGill, and T. D. Irgang, 1995: Visible wavelength Doppler lidar for measurement of wind and aerosol profiles during day and night, *Opt. Eng*., **34**, 499–511.

Garnier, A. and M. L. Chanin, 1992: Description of a Doppler Rayleigh LIDAR for measuring winds in the middle atmosphere, *Appl. Phys*., **55**, 35–40.

Gentry, B. and C. L. Korb, 1994: Edge technique for high accuracy Doppler velocimetry, *Appl. Opt*., **33**, 5770–5777.

Grund C. J., and E.W. Eloranta, 1991: University of Wisconsin high spectral resolution lidar. *Opt. Eng*., **30**, 6–12.

Hair, J. W., and Coauthors, 2008: Airborne High Spectral Resolution Lidar for profiling aerosol optical properties. *Appl. Opt.*, **47,** 6734–6752.

Hall Jr., F. F., R. M. Huffaker, R. M. Hardesty, M. E. Jackson, T. R. Lawrence, M. J. Post, R. A. Richter, and B. F. Weber, 1984: Wind measurement accuracy of the NOAA pulsed infrared Doppler lidar, *Appl. Opt*., **23**, 2503–2506.

Hovis, F.E. , M. Rhoades, R. L. Burnham, J. D. Force, T. Schum, B. M. Gentry, H. Chen, S. X. Li, J. W. Hair, A. L. Cook, and C. A. Hostetler, 2004: Single-frequency lasers for remote sensing. Proc. SPIE 5332, 263–270.

Huffaker, R. M., T. R. Lawrence, M. J. Post, J. T. Priestly, F. F. Hall Jr., R. A. Richter, and R. J. Keeler, 1984: Feasibility studies for a global wind measuring satellite system Windsat: analysis of simulated performance, *Appl. Opt.,* **23**, 2532–2536.

Jensen, E. J., Lawson, P., Baker, B., Pilson, B., Mo, Q., Heymsfield, A. J., Bansemer, A., Bui, T. P., McGill, M., Hlavka, D., Heymsfield, G., Platnick, S., Arnold, G. T., and Tanelli, S., 2009: On the importance of small ice crystals in tropical anvil cirrus, Atmos. Chem. Phys., 9, 5519-5537, doi:10.5194/acp-9-5519-2009.

Klett, J. D., 1981: Stable analytical inversion solution for processing lidar returns. *Appl. Opt*, **20**, 211–220.

Klett, J. D., 1985: Lidar inversion with variable backscatter/extinction ratios. *Appl. Opt*, **24**, 1638–1643.

Lee, W.C., P. Dodge, F.D. Marks, P.H. Hildebrand, 1994: Mapping of airborne Doppler radar data, *J. Atmos. Oceanic Technol.*, **11**, 572–578.

Leon, D., and G. Vali, 1998: Retrieval of Three-Dimensional Particle Velocity from Airborne Doppler Radar Data, *J. Atmos. Oceanic Technol.*, **15**, 860–870.

McGill, M.J., 1996: Recovery and Validation of Wind and Aerosol Profiles from Incoherent Doppler Lidar Measurements. PhD Thesis, University of Michigan (Ann Arbor, MI).

McGill, M. J., W. R. Skinner, and T. D. Irgang, 1997a: Analysis techniques for the recovery of winds and backscatter coefficients from a multiple channel incoherent Doppler lidar, *Appl. Opt*., **36**, 1253–1268.

McGill, M. J., W. R. Skinner, and T. D. Irgang, 1997b: Validation of wind profiles measured using incoherent Doppler lidar, *Appl. Opt*., **36**, 1928–1939.

McGill, M. J., M. Marzouk, V. S. Scott, and J. D. Spinhirne, 1997c: Holographic circle-to-point converter with particular applications for lidar work, *Opt. Eng*., **36**, 2171–2175.

McGill, M.J., and J.D. Spinhirne, 1998: Comparison of two direct-detection Doppler lidar techniques, *Opt. Eng*., **37**, 2675–2686.

McGill, M.J., and R.D. Rallison, 2001: Holographic optics convert rings to points for Detection. *Laser Focus World*, **37**, 131-136.

McGill, M. J., D. Hlavka, W. Hart, V. S. Scott, J. Spinhirne, and B. Schmid, 2002: Cloud Physics Lidar: instrument description and initial measurement results. *Applied Optics*, **41**, 3725-3734.

McGill, M. J., M. A. Vaughan, C. R. Trepte, W. D. Hart, D. L. Hlavka, D. M. Winker, and R. Kuehn, 2007: Airborne validation of spatial properties measured by the CALIPSO lidar. *J. Geophys. Res*., **112**, D20201, doi:10.1029/2007JD008768.

McGill, Matthew, Thorsten Markus, V. Stanley Scott, Thomas Neumann, 2013: The Multiple Altimeter Beam Experimental Lidar (MABEL): An Airborne Simulator for the ICESat-2 Mission. *J. Atmos. Oceanic Technol.*, 30, 345–352. doi: http://dx.doi.org/10.1175/JTECH-D-12-00076.1

Piironen P. and E.W. Eloranta, 1994: Demonstration of a high-spectral-resolution lidar based on an iodine absorption filter. *Opt. Lett*., **19**, 234–236.

Russell, P. B., T. J. Swissler, and M. P. McCormick, 1979: Methodology for error analysis and simulation of lidar aerosol measurements, Appl. Opt., 18, 3783–3797.

Schwiesow, R.L., F. Köpp, and C. Werner, 1985: Comparison of Lidar-Measured Wind Values Obtained by Full Conical Scan, Conical Sector Scan, and Two Point Techniques, *J. Atmos. Oceanic Technol*., **2**, 3.

Shipley, S. T., D. H. Tracy, E. W. Eloranta, J. T. Tauger, J. T. Sroga, F. L. Roesler, and J. A. Weinman, 1983: High spectral resolution lidar to measure optical scattering properties of atmospheric aerosols. 1: Theory and instrumentation. *Appl. Opt*., **22**, 3716–3724.

Spinhirne, J. D., S. P. Palm, W. D. Hart, D. L. Hlavka, and E. J. Welton, 2005: Cloud and aerosol measurements from GLAS: Overview and initial results. Geophys. Res. Lett., **32**, L22S03, doi:10.1029/2005GL023507.

Tenti, G., C. D. Boley, and R. C. Desai, 1974: On the kinetic model description of Rayleigh–Brillouin scattering from molecular gases. *Can. J. Phys*, **52**, 285–290.

Vaughan, M.A., Z. Liu, M.J. McGill, and M.D. Obland, 2010: On the spectral dependence of backscatter from cirrus clouds: an assessment of CALIOP's 1064 nm calibration using Cloud Physics Lidar measurements, *Atmospheric Chemistry and Physics*.

Werner, C., 2005: "Doppler Wind Lidar," in *Lidar: Range-Resolved Optical Remote Sensing of the Atmosphere*, C. Weitkamp, ed. (Springer), 325-354.

Whiteman, D. N., B. Demoz, and Z. Wang, 2004: Subtropical cirrus cloud extinction to backscatter ratios measured by Raman Lidar during CAMEX-3. *Geophys. Res. Lett*., **31**, L12105, doi:10.1029/2004GL020003.

Winker, D. M., M. A. Vaughan, A. H. Omar, Y. Hu, K. A. Powell, Z. Liu, W. H. Hunt, and S. A. Young, 2009: Overview of the CALIPSO Mission and CALIOP Data Processing Algorithms. *J. Atmos. Oceanic Technol*., **26**, 1105-1119, doi:10.1175/2009JTECHA1281.1.

Yorks, J. E., D. L. Hlavka, W. D. Hart, M. J. McGill, 2011a: Statistics of Cloud Optical Properties from Airborne Lidar Measurements. *J. Atmos. Oceanic Technol.*, **28**, 869–883. doi: http://dx.doi.org/10.1175/2011JTECHA1507.1

Yorks, J. E., D. L. Hlavka, M. A. Vaughan, M. J. McGill, W. D. Hart, S. Rodier, and R. Kuehn, 2011b: Airborne validation of cirrus cloud properties derived from CALIPSO lidar measurements: Spatial properties, *J. Geophys. Res*., **116**, D19207, doi:10.1029/2011JD015942.

Young, A.T., 1981: Rayleigh scattering. *Phys. Today*, **35**, 42–48.

Young, S. A., and M. A. Vaughan, 2009: The retrieval of profiles of particulate extinction from Cloud-Aerosol Lidar Infrared Pathfinder Satellite Observations (CALIPSO) data: Algorithm description. *J. Atmos. Oceanic Technol.*, **26**, 1105–1119.

Young, Stuart A., Mark A. Vaughan, Ralph E. Kuehn, David M. Winker, 2013: The Retrieval of Profiles of Particulate Extinction from Cloud–Aerosol Lidar and Infrared Pathfinder Satellite Observations (CALIPSO) Data: Uncertainty and Error Sensitivity Analyses. *J. Atmos. Oceanic Technol.*, **30**, 395–428. doi: http://dx.doi.org/10.1175/JTECH-D-12-00046.1

Zhao, Y., G. G. Mace, and J. M. Comstock, 2011: The occurrence of particle size distribution bimodality in midlatitude cirrus as inferred from ground-based remote sensing data, *J. Atmos. Sci*., **68**, 1162–1177, doi:10.1175/2010JAS3354.1.

Table 1. Primary system parameters for ACATS lidar.

Parameter	Value
Laser Type	Nd: YAG, seeded
Wavelength	532 nm
Laser Repetition Rate	250 Hz
Laser Output Energy	~10 mJ/pulse
Telescope Diameter	8 inches
Viewing Angle	45 degrees
Telescope FOV	350 μradians (full angle)
Bandpass Filter	150 pm FWHH
Etalon Spacing	10 cm
Etalon Reflectivity	85%
Orders Imaged	1.2
Detector Channels	24
Raw Range Resolution	30 m
Horizontal Resolution	1 sec (~200 m)
Platform Speed	~200 m/s
Platform Altitude	~ 20 km (65,000 ft)

Table 2. Definitions of parameters found in the ACATS lidar equation

Variable	Definition	Units
N(r)	number of photons detected per range bin	-
r	distance to the scattering particle	m
j	detector channel	-
E_T	transmitted laser energy	J
λ	laser wavelength	m
h	Planck's constant	J sec
c	speed of light	m s^{-1}
A_T	area of lidar telescope	m^2
Δr	range bin width	m
Q_E	detector quantum efficiency	-
T_O	system optical efficiency	-
T_F	optical filter efficiency	-
$O_A(r)$	overlap function	-
n_c	number of detector channels	-
η_c	detector normalization	-
N_{FSR}	free spectral range (channel number)	-
$\Delta\lambda_{FSR}$	free spectral range (wavelength)	m^{-1}
$\Delta\lambda_L$	laser broadening 1/e width (wavelength)	m^{-1}
$\Delta\lambda_M$	molecular broadening 1/e width (wavelength)	m^{-1}
$\alpha(r)$	attenuated particulate backscatter coefficient	m^{-1} sr^{-1}
$\omega(r)$	attenuated molecular backscatter coefficient	m^{-1} sr^{-1}
φ	off-nadir pointing angle	degrees
U_{LOS}	LOS wind velocity	m s^{-1}
λ_c	center position of the laser linewidth	m
λ_c	center wavelength of the etalon	m

Figures

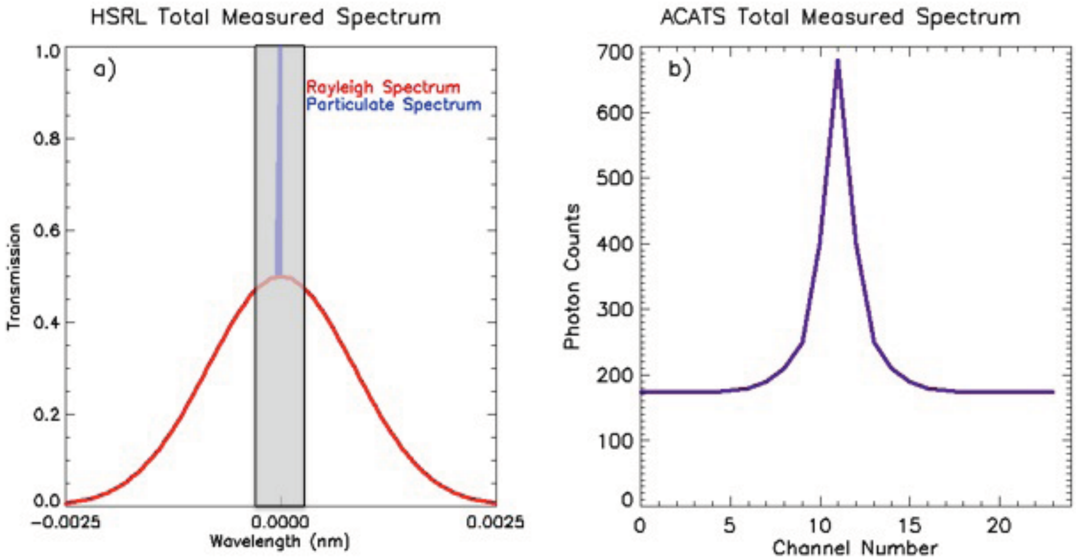

Figure 1. The ACATS method images the grey shaded area of the returned atmospheric signal (a) onto a 24 channel array detector, which measures the photon counts at each wavelength interval independently as a total backscattered signal (b).

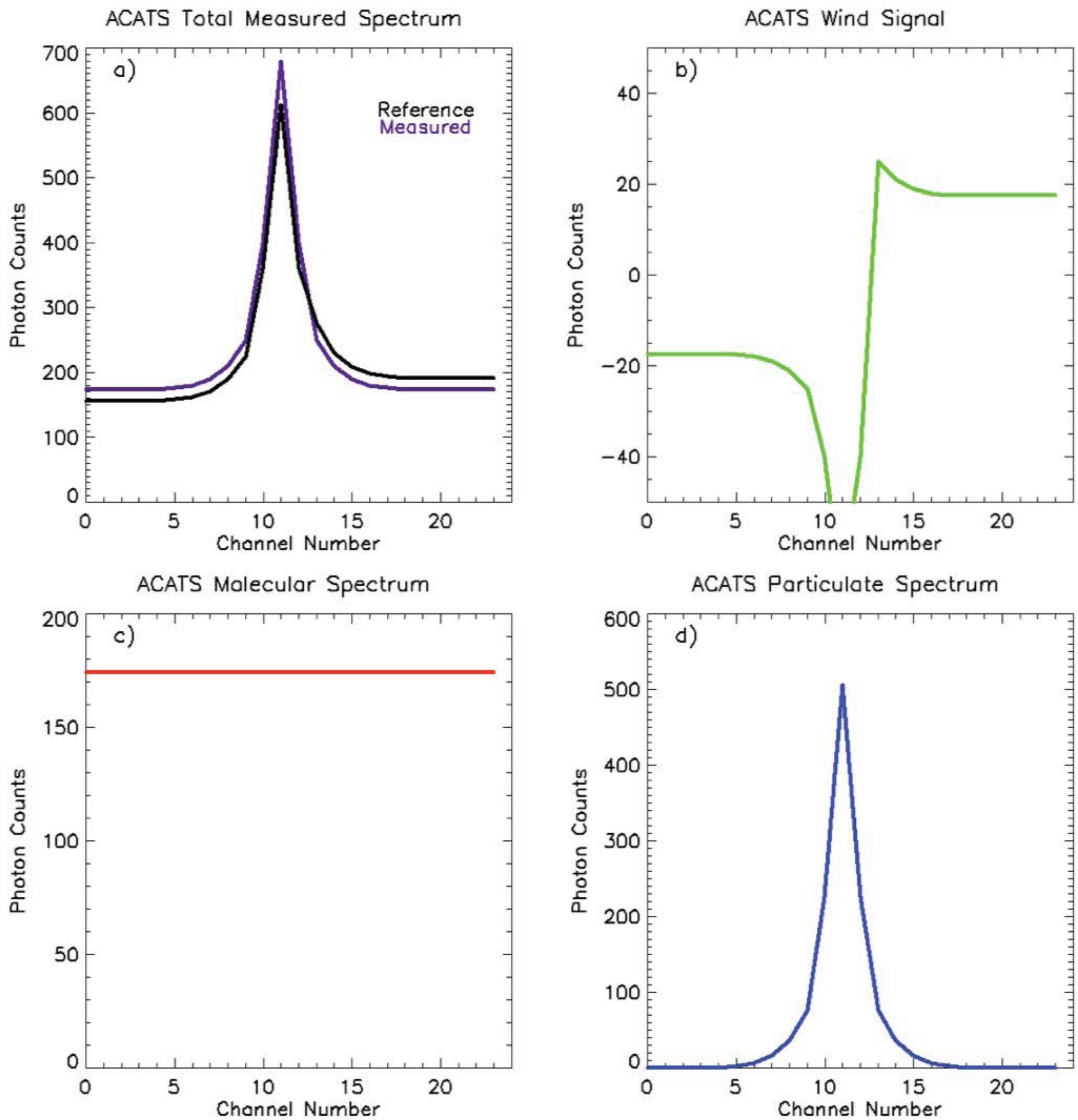

Figure 2. The Doppler shifted atmospheric signal (purple) measured by ACATS is compared to an unshifted reference spectrum (a), which yields the Doppler wind signal (b) of the ACATS measurement. The broad Rayleigh scattered spectrum (c) is measured by ACATS as a nearly flat background of the total atmospheric return signal, resulting in a sharp particulate spectrum (d) that is directly measured.

Figure 3. The fully assembled ACATS instrument (a) includes the receiver tube covered in insulation (left) and a pressurized telescope dome (right). A picture of the inside of the receiver subsystem (b) shows the etalon (silver device in the middle), the 24-channel array detector, and circle-to-point converter. The inside of the telescope subsystem (c) contains a motor to rotate the telescope and a HOE.

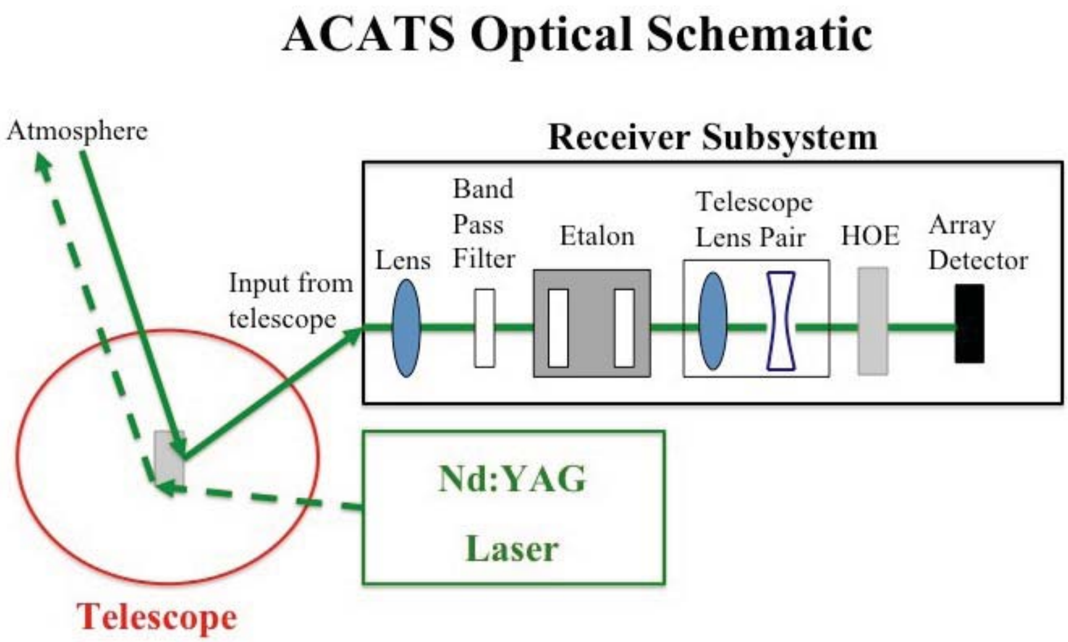

Figure 4. The ACATS optical schematic shows the outgoing 532 nm laser light (dashed green), originating from the Nd:YAG laser, directed out of the telescope by a mirror. The return signal (solid green) is passed through the telescope and into the receiver subsystem using an optical fiber, where it is transmitted through optical lenses and filters, including the etalon.

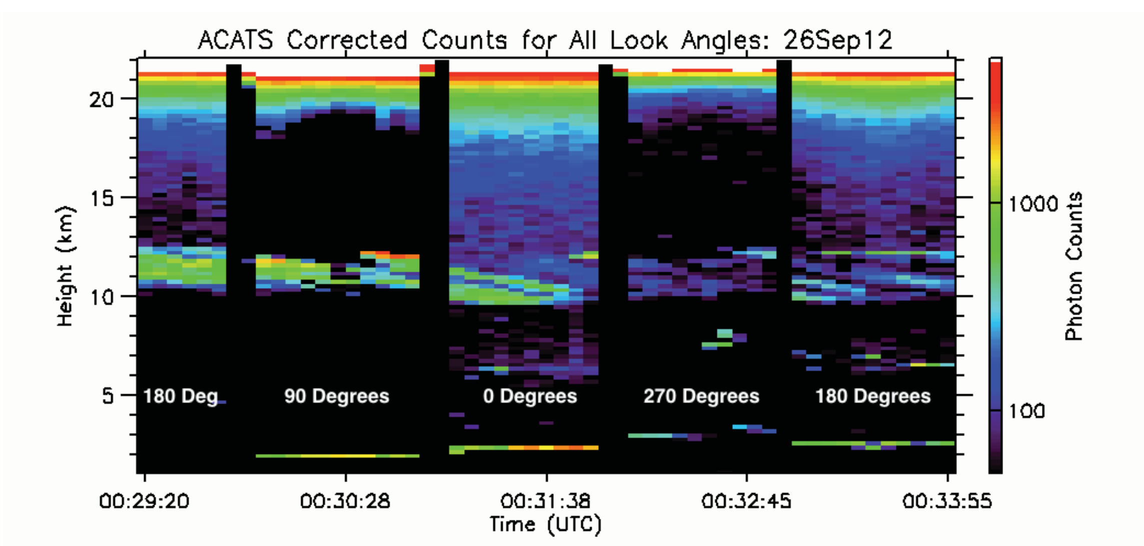

Figure 5. ACATS photon counts from an ER-2 flight on 26 September 2012. The high count rates between 10 and 12 km show the detection of a cirrus layer at all four look angles at intervals of 60 seconds.

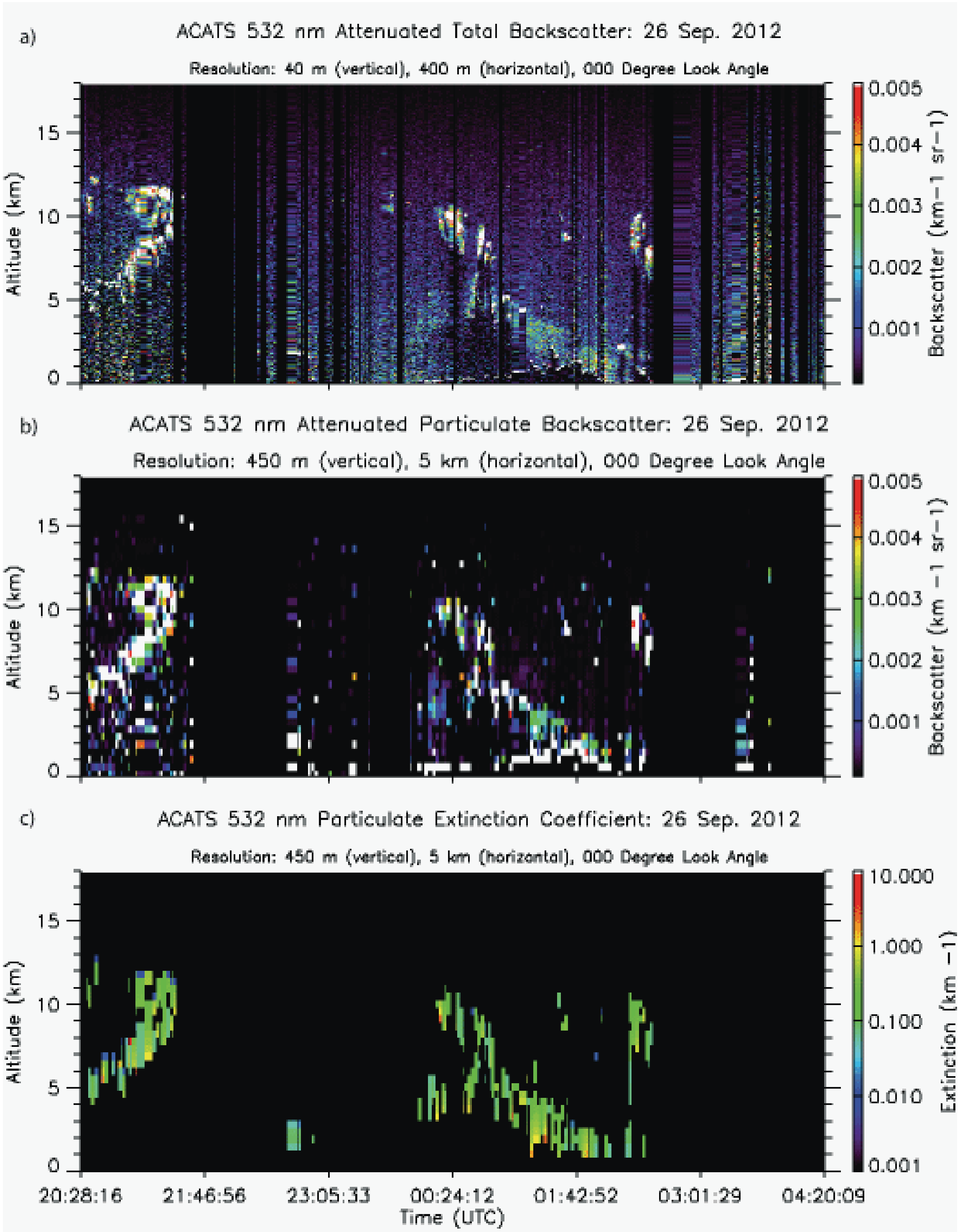

Figure 6. The ACATS 532 nm Attenuated Total Backscatter (km^{-1} sr^{-1}) computed using the standard method (a), the Attenuated Particulate Backscatter (km^{-1} sr^{-1}) derived using the HSRL method (b), and the directly-retrieved Particulate Extinction Coefficient (km^{-1}) at the 0 degree look angle (c) for the ER-2 flight on 26 September. ACATS observed clouds as the ER-2 flew over the Ohio River Valley (20:28:05 to 21:30:00 UTC) and a large smoke plume (00:24:10 to 02:10:00 UTC) that extended as high as 6 km over Montana.

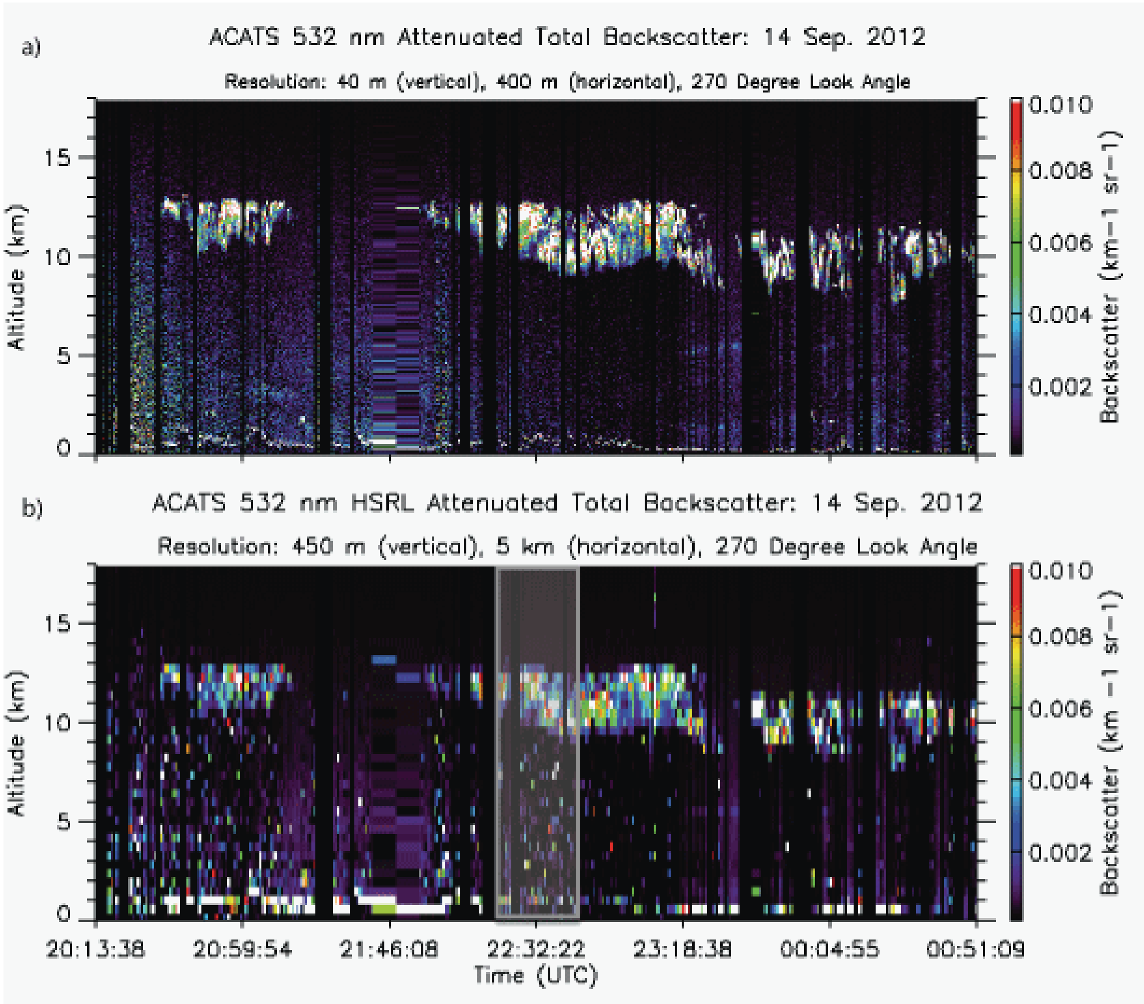

Figure 7. The ACATS 532 nm Attenuated Total Backscatter computed using the standard method (a) and using the HSRL method (b) at the 270 degree look angle for the ER-2 flight on 14 September. The grey box focuses on a 35 minute segment in which the mean profiles are compared in Figure 8 for cirrus clouds.

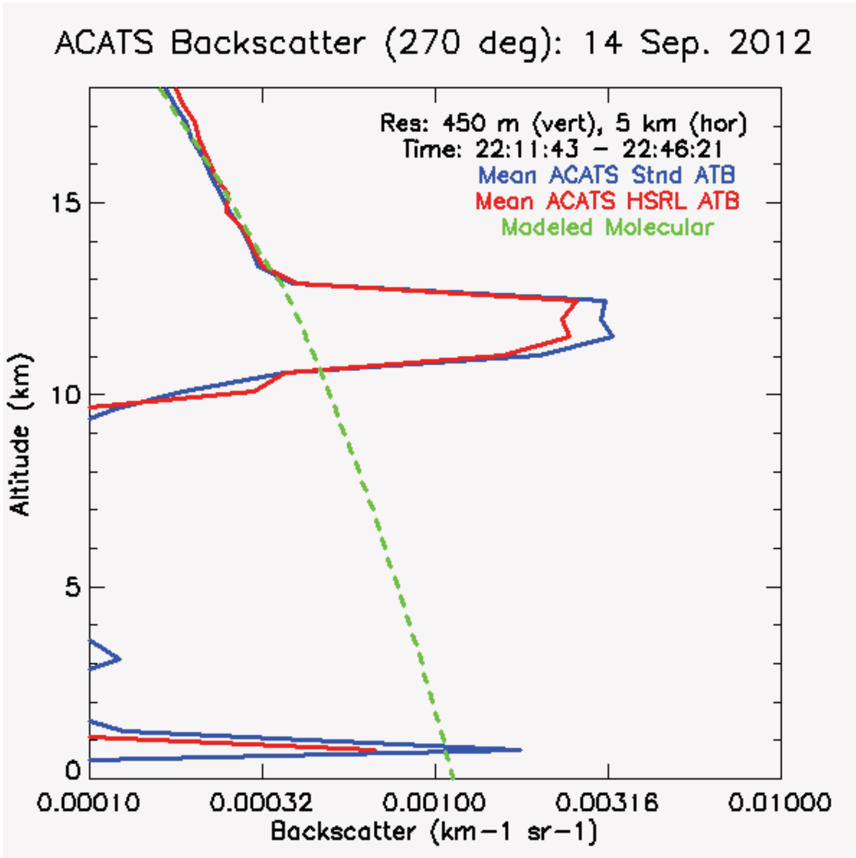

Figure 8. The ACATS mean profiles of 532 nm Attenuated Total Backscatter computed using the standard method (blue) averaged to the resolutions of the HSRL products, as well as the Attenuated Total Backscatter using the HSRL method (red) for the grey shaded box in Figure 7b (22:11:43 – 22:46:21 UTC).